Inorganic Chemistry

Article

pubs.acs.org/IC

The Trivalent Copper Complex of a Conjugated Bis-dithiocarbazate Schiff Base: Stabilization of Cu in Three Different Oxidation States

Mohammad Akbar Ali,[†] Paul V. Bernhardt,*[,‡] Mathilde A. H. Brax,[‡] Jason England,[§] Anthony J. Farlow,[‡] Graeme R. Hanson,[∥] Lee Len Yeng,[†] Aminul Huq Mirza,[†] and Karl Wieghardt[§]

[†]Chemistry Programme, Faculty of Science, Universiti Brunei Darussalam, BE 1410, Brunei Darussalam

[‡]School of Chemistry and Molecular Biosciences, The University of Queensland, Brisbane, 4072, Australia

[§]Max Planck Institute for Chemical Energy Conversion, Stiftstrasse 34-36, 45470 Mülheim an der Ruhr, Germany

[∥]Centre for Advanced Imaging, The University of Queensland, Brisbane, 4072, Australia

Supporting Information

ABSTRACT: The new tribasic N_2S_2 ligand H_3ttfasbz has been synthesized by condensation of 4-thenoyl 2,2,2-trifluoroacetone and *S*-benzyl dithiocarbazate. On complexation with copper(II) acetate, spontaneous oxidation to the Cu^{III} oxidation state is observed, and the complex [Cu(ttfasbz)] has been isolated and characterized structurally. Reduction to the EPR active Cu^{II} analogue has been achieved chemically and also electrochemically, and in both cases, the process is totally reversible. The $Cu^{III/II}$ redox potential of the complex is remarkably low and similar to that of the ferrocenium/ferrocene couple. Further reduction to the formally monovalent (d^{10}) dianion $[Cu^{I}(ttfasbz)]^{2-}$ may be achieved electrochemically. Computational chemistry demonstrates that the three redox states [Cu(ttfasbz)], $[Cu(ttfasbz)]^{-}$, and $[Cu(ttfasbz)]^{2-}$ are truly Cu^{III}, Cu^{II}, and Cu^{I} complexes, respectively, and the potentially noninnocent ligand does not undergo any redox reactions.

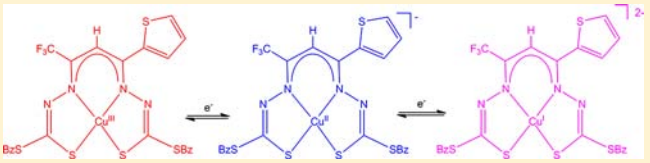

INTRODUCTION

Although still an unusually high oxidation, a number of trivalent copper complexes are now well characterized. Typically, two or more ligand donor atoms in the Cu^{III} complex are formally anionic, which compensates for the high positive charge of the metal. The types of ligands that are known to stabilize trivalent copper include N-deprotonated oligopeptides,[1−4] N-confused porphyrins,[5] corroles,[6,7] oxamates,[8] thiolates,[9] and also various N-deprotonated amido[10] and mixed donor amido/thiolate ligands.[8,11−13] In all cases, the ligands are weak acids and are deprotonated (as di-, tri-, or tetraanions) upon coordination. As all of these ligands also possess unsaturated and delocalized electronic structures, a clear definition of the metal oxidation state is not straightforward. This is generally termed ligand noninnocence,[14,15] where redox reactions of the organic ligand may be coupled with reactions on the metal center. Computational chemistry has proven effective in defining the exact nature of the electronic ground state and thus providing an accurate picture of the *d* electronic configuration.[15−17]

A particularly unusual class of ligands is based on acetylacetone (pentane-2,4-dione) bis-*S*-alkyl-isothiosemicarbazone (Chart 1). Ligands from this family, for example, the *S*-methyl analogue acasme^{3-}, bind as planar, trianionic, tetradentate N-donors and have been found to stabilize Cu^{III} as well as Fe^{IV} complexes.[11,18] However, the trianions (in their coordinated form) were shown to be noninnocent and could also exist in a two-electron oxidized (monoanionic) form based on structural and spectroscopic evidence.[19] A structurally related compound is the *S*-benzyldithiocarbazate derivative of the *β*-diketone 4-thenoyl-2,2,2-trifluoroacetone, which, in its trianionic form (ttfasbz^{3-}), shares many of the features of acasme^{3-} but bears an N_2S_2 set of donor atoms. Herein, we report the Cu coordination chemistry of this new ligand.

Chart 1

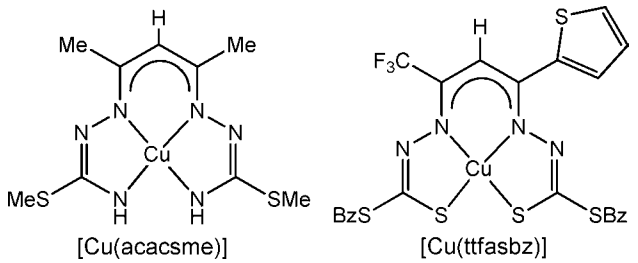

EXPERIMENTAL SECTION

Syntheses. *S*-Benzyl dithiocarbazate was synthesized as previously described.[20] All other reagents were AR grade and were obtained commercially.

H_3ttfasbz. Solid 4-thenoyl-2,2,2-trifluoroacetone (0.64 g, 2.88 mmol) was added to a solution of *S*-benzyl dithiocarbazate (1.13 g, 5.70 mmol) in hot EtOH (25 mL). The mixture was refluxed for 24 h. The mixture was cooled to room temperature, and an off-white

Received: November 27, 2012
Published: January 16, 2013

   dx.doi.org/10.1021/ic302596h | *Inorg. Chem.* 2013, 52, 1650−1657

precipitate was filtered off and washed with a small volume of cold EtOH (0.17 g, 10%); mp 180−184 °C. Anal. calcd for $C_{24}H_{21}F_3N_4S_5$: C, 49.47; H, 3.63; N, 9.61. Found: C, 49.5; H, 3.6; N, 9.6%. ^{1}H NMR (DMSO-d_6) δ: 3.55 and 4.18 (AB q, 2H); 4.37 (q, 2H); 4.42 (q, 2H); 7.2−7.5 (m, 11H); 7.74 (d, 1H); 7.88 (d, 1H); 8.02 (s, 1H), 11.64 (s, 1H). ^{13}C NMR (DMSO-d_6) δ: 37.8, 38.3, 88.0 (q, CF_3), 121.1, 124.9, 127.3, 127.4, 128.5, 128.6, 128.7, 129.2, 129.5, 131.4, 132.3, 133.6, 135.6, 136.7, 149.9, 194.2, 204.5.

[Cu^{III}(ttfasbz)]. The ligand H_3ttfasbz (50 mg; 120 μmol) was dissolved in boiling abs. ethanol (15 mL) and combined with a hot solution of copper(II) acetate hydrate (30 mg; 120 μmol) in EtOH (50 mL). The mixture was heated on a water bath for ca. 10 min. The reaction mixture was left to stand for about 3 days whereupon the product that had formed was filtered off, washed with abs. ethanol, and dried in a desiccator over anhydrous silica gel. Yield, 3.6 mg (4%). Anal. calcd for $C_{24}H_{24}CuF_3N_4O_{2.5}N_4S_5$: C, 41.82, H, 3.51; N, 8.12%. Found: C, 41.5; H, 2.6; N, 8.0. IR (cm^{-1}): 1662s, 1654s, 1560s, 1508s, 1414s, 1350s, 1314s, 1129s, 993s. Crystals suitable for X-ray work were obtained by slow evaporation of a MeCN solution of the complex.

Physical Methods. Cyclic voltammetry was performed on a BAS100B/W potentiostat employing a glassy carbon working electrode, Pt auxiliary electrode, and Ag/AgCl reference electrode. The supporting electrolyte was 0.1 $NaNO_3$, and all solutions were purged with Ar before measurement. IR spectra were measured. ^{1}H and ^{13}C NMR spectra were recorded on a Varian Unity-300 (300 MHz ^{1}H, 75 MHz ^{13}C) spectrometer in DMSO-d_6.

EPR Spectroscopy. Multifrequency (X- and S-band) electron paramagnetic resonance (EPR) spectra were measured with a Bruker Elexsys E500 EPR spectrometer equipped with an EIP microwave frequency counter and a Bruker ER034 M Teslameter for calibration of the microwave frequency and magnetic field, respectively. Low temperatures were achieved at the sample position in the super high Q-cavity using a Bruker nitrogen flow through system in conjunction with a Eurotherm temperature controller. Room temperature X-band EPR spectra employed the same cavity but utilized an AquaX cell to minimize dielectric loss from the DMF solvent. At S-band frequencies, normal 3 mm ID quartz EPR tubes were inserted into a flexline split ring resonator. Samples for EPR measurements at both room and low temperatures were prepared as 1 mM DMF solutions. Spin Hamiltonian and line width parameters were determined by spectral simulation with the program XSophe-Sophe-XeprView running on a personal computer with Mandriva Linux 2010.2 as the operating system.[21] A Kivelson line width model[22−25] ($\sigma = \alpha + \beta M_I + \gamma M_I^2 + \delta M_I^3$) was used for the simulation of the isotropic room temperature spectra measured at both X-band (α = 9.04, β = 4.51, γ = 1.20, and δ = −0.086) and S-band (α = 8.70, β = 2.51, γ = 2.23, and δ = −0.0364) microwave frequencies. For the X-band anisotropic frozen solution spectrum, a Hyde−Froncisz distribution of g and A values[26,27] [$\sigma_v^2 = \Sigma_{i=x,y,z}$ ($\sigma R_i^2 + (\sigma g_i^2/g_i^2 + \sigma A_i M_I)^2$)] was used to simulate the variation of line width (σR_i = 1.24, 0.0, 2.31; $\sigma g_i/g_i$ = 0.000611, 0.00171, 0.00155; σA_i = −2.033, 2.632, 0.240 × 10^{-4} cm^{-1}; and $i = x, y, z$) as a function of the nuclear spin quantum number (M_I) and resonant fields.

Crystallography. X-ray data were collected on an Oxford Diffraction Gemini CCD diffractometer employing graphite-monochromated Mo Kα radiation (0.71073 Å) and operating within the range $2 < 2\theta < 50$ Å. Data reduction and empirical absorption corrections (multiscan) were performed with Oxford Diffraction CrysAlisPro software (Oxford Diffraction, vers. 171.36.21). The structure was solved by direct methods with SHELXS and refined by full-matrix least-squares analysis with SHELXL-97.[28] All non-H atoms were refined with anisotropic thermal parameters. The molecular structure diagram was produced with ORTEP3.[29] Crystal data are given in Table 1.

DFT Calculations. All DFT calculations were performed using the ORCA software package.[30] The geometry optimizations of all complexes and single-point calculations using the atomic coordinates of the optimized geometries and X-ray crystal structures were carried out using the B3LYP functional.[31−33] In all calculations, def2-TZVP basis sets were applied to all atoms.[34] Auxiliary basis sets used to expand the electron density in the calculations were chosen to match the orbital basis.[35,36] The RIJCOSX[37,38] approximation was used to accelerate the calculations. The authenticity of each converged structure was confirmed by the absence of imaginary vibrational frequencies. Use of the Conductor-like Screening Model (COSMO),[39] with DMF as the solvent, and the empirical dispersion forces correction vdw06[40] had little impact of the electronic structures of the various calculated states relative to their gas phase counterparts. Hence, all discussions herein are based on the latter.

The self-consistent field calculations were tightly converged (1 × 10^{-8} E_h in energy, 1 × 10^{-7} E_h in the density change, and 1 × 10^{-7} in maximum element of the DIIS error vector). The geometry optimizations for all complexes were carried out in redundant internal coordinates without imposing symmetry constraints. In all cases, the geometries were considered converged after the energy change was less than 5 × 10^{-6} E_h, the gradient norm and maximum gradient element were smaller than 1 × 10^{-4} E_h Bohr^{-1} and 3 × 10^{-4} E_h Bohr^{-1}, respectively, and the root-mean square and maximum displacements of all atoms were smaller than 2 × 10^{-3} and 4 × 10^{-3} Bohr, respectively.

In this paper, we describe our computational results by using the BS approach pioneered by Noodleman et al.[41] Given that several broken-symmetry solutions to the spin-unrestricted Kohn−Sham equations may be obtained, the general notation BS(m,n)[42] has been adopted, where m(n) denotes the number of spin-up (spin-down) electrons at the two interacting fragments. Canonical and corresponding orbitals[43] as well as spin density plots were generated with the program Chimera.[44]

Table 1. Crystal Data for [Cu(ttfasbz)]

formula	$C_{24}H_{18}CuF_3N_4S_5$
Fw	643.26
cryst syst	triclinic
space group	$P\bar{1}$ (no. 2)
a (Å)	5.0358(3)
b (Å)	13.267(1)
c (Å)	20.367(1)
α (°)	87.617(5)
β (°)	85.132(4)
γ (°)	79.557(5)
V (Å^3)	1332.9(1)
Z	2
T (K)	293(2)
λ (Å)	0.71073
μ (cm^{-1})	1.254
ρ_{calcd}	1.603
R (obs data)[a]	0.0377
wR_2 (all data)[b]	0.0601

[a] $R(F_o) = \Sigma||F_o| - |F_c||/\Sigma|F_o|$. [b] $R_w(F_o^2) = [\Sigma\, w(F_o^2 - F_c^2)/\Sigma wF_o^2]^{1/2}$.

RESULTS AND DISCUSSION

Ligand Synthesis. The Schiff base condensation reaction (Scheme 1) between 2-thenoyltrifluoroactone (**A**, which exists primarily as the enol tautomer in solution) and 2 equiv of *S*-benzyl-dithiocarbazate does not lead to the open chain di-imine **C**, but instead, the asymmetric pyrazoline (**E**) was obtained. Intramolecular nucleophilic attack by the (deprotonated) NH group occurs exclusively at the more electrophilic C-atom adjacent to the $-CF_3$ group (**D**, in the *E*-isomeric form). The yield of this product is rather poor relative to similar condensation reactions[45−47] despite many attempts using alternative solvents and reaction conditions. The monoimine (**B**), which exists as the keto tautomer in DMSO and in the solid state,[48] was commonly a major product. The progress of the reaction was followed by TLC, and a mixture of compounds

dx.doi.org/10.1021/ic302596h | Inorg. Chem. 2013, 52, 1650−1657

Scheme 1. Formation of the Cyclic Product H_3ttfasbz

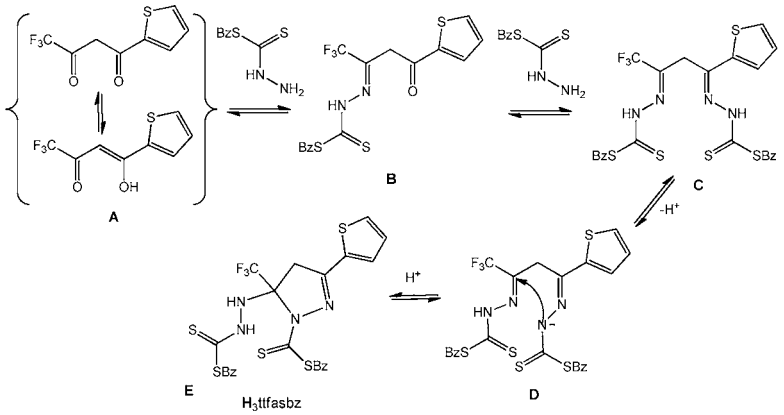

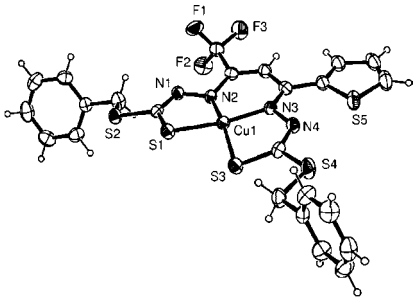

Figure 1. ORTEP molecular structure of [Cu^{III}(ttfasbz)]. Selected bond lengths (Å) and angles (°): N2−Cu, 1.897(2); N3−Cu, 1.909(2); S1−Cu, 2.1802(9); S3−Cu, 2.1769(9); N2−Cu−N3, 96.7(1); N2−Cu−S3, 166.41(8); N2−Cu−S1, 87.75(8); and S3−Cu−S1, 89.49(3).

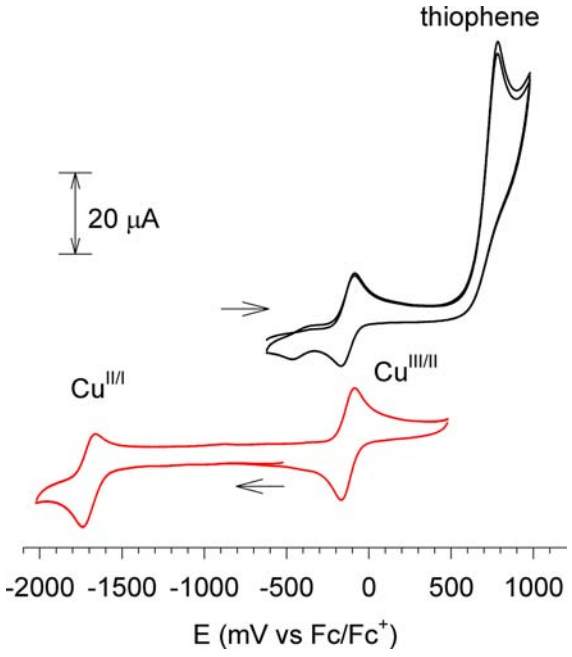

Figure 2. Cyclic voltammetry of [Cu(ttfasbz)] (1 mM in DMF and 0.1 M Et_4NClO_4). Working electrode glassy carbon; sweep rate 100 mV/s. Upper trace confined to the window −600 < E < +1000 mV, while the lower trace is within the window −2000 < E < +500 mV vs $Fc^{+/0}$. Arrows indicate the initial direction of sweep.

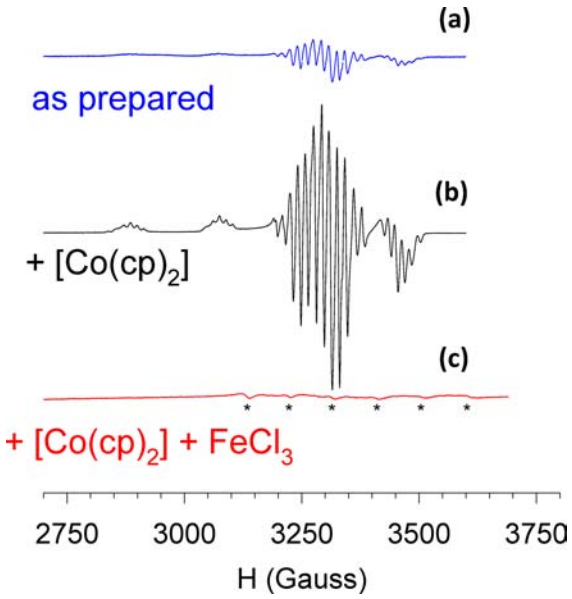

Figure 3. X-band (9.449 GHz) frozen solution (1 mM in DMF) EPR spectra (130 K) of (a) [Cu^{III}(ttfasbz)] as prepared (partically reduced by the solvent), (b) [Cu^{III}(ttfasbz)] reduced with cobaltocene to its monoanion [Cu^{II}(ttfasbz)]$^-$, and (c) fully reoxidized with $FeCl_3$ (bottom). The resonances labeled with a "*" arise from Mn^{II} impurities in the $FeCl_3$ oxidant.

was present in solution even after 24 h of reflux. The pyrazoline H_3ttfasbz precipitates from EtOH at room temperature, enabling its separation from the other components.

^{1}H and ^{13}C NMR clearly discriminate the cyclic pyrazoline **E** from its open chain isomer **C**. The methylene protons in isomer **C** are necessarily equivalent due to the planar symmetry of this molecule, so yield a single ^{1}H NMR resonance. In the pyrazoline **E**, the rigidity of the five-membered ring results in an AB quartet from the now inequivalent methylene protons. This is evident in the ^{1}H NMR spectrum (AB doublets at 3.55, 4.18 ppm). The remaining peaks are due to the nonequivalent *S*-benzyl methylenes and the three thiophene protons. A similar cyclization reaction has been reported for analogous *S*-methyl dithiocarbazate in reaction with other *β*-diketones.[45,47]

Copper Complexation. Reaction of H_3ttfasbz with (divalent) [$Cu(OAc)_2$] in EtOH led to the neutral complex [Cu(ttfasbz)]. Given that the ligand is a tribasic acid, this formally corresponds to trivalent copper. Crystals suitable for X-ray studies were obtained, and the crystal structure of the

dx.doi.org/10.1021/ic302596h | Inorg. Chem. 2013, 52, 1650−1657

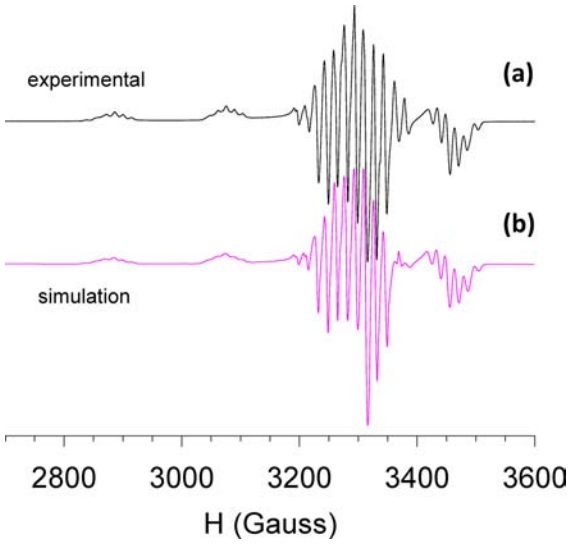

Figure 4. Experimental (a) and simulated (b) X-band (9.343 GHz) EPR spectra (1 mM in DMF, 130 K) of $[Cu^{II}(ttfasbz)]^-$ prepared by reduction of the parent Cu^{III} complex with cobaltocene.

complex is shown in Figure 1. The coordination geometry is distorted square planar with no other contacts to the metal ion perpendicular to the CuN_2S_2 plane closer than 3.55 Å. The Cu−N (∼1.90 Å) and Cu−S (∼2.18 Å) bonds in this structure are significantly shorter than typical Cu^{II} N_2S_2 complexes of related ligands (Cu^{II}−N ∼1.94−1.98 Å and Cu^{II}−S ∼2.24 Å)[49−51] and are consistent with the few known comparable Cu^{III} complexes.[11,12] These two features (square planar geometry and short coordinate bonds) both suggest a low spin d^8 ground state akin to isoelectronic and more common square planar Ni^{II} complexes. The three chelate rings defined by the tetradentate coordinated ligand are close to planar. The least-squares plane defined by the ligand backbone (comprising the continuous chain of non-H atoms from S2 to S3 inclusive) reveals a modest tetrahedral distortion of the CuN_2S_2 moiety with *trans* pairs of donor atoms lying on the same side of the best plane as each other: S1 (+0.326 Å) and N3 (+0.121 Å) and S3 (−0.272 Å) and N2 (−0.215 Å). The two benzyl groups adopt different orientations (syn/anti) with respect to their adjacent coordinated S-donor.

Most importantly, all H-atoms were clearly resolved in difference electron density maps, and the three sites of deprotonation (taking structure **C** in Scheme 1 as a starting point) were unambiguously defined as the two noncoordinated N-atoms (N1 and N4) and the apical methylene bridging the two imine functional groups. Deprotonation of both thioamide N-atoms (N1 and N4) is typical in dithiocarbazate Schiff base coordination chemistry as well as related thiosemicarbazone

Chart 2

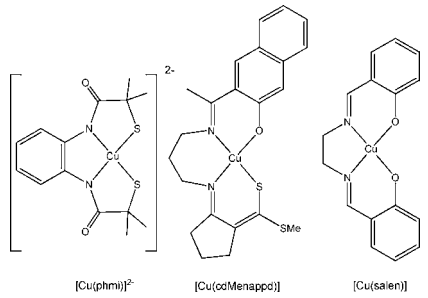

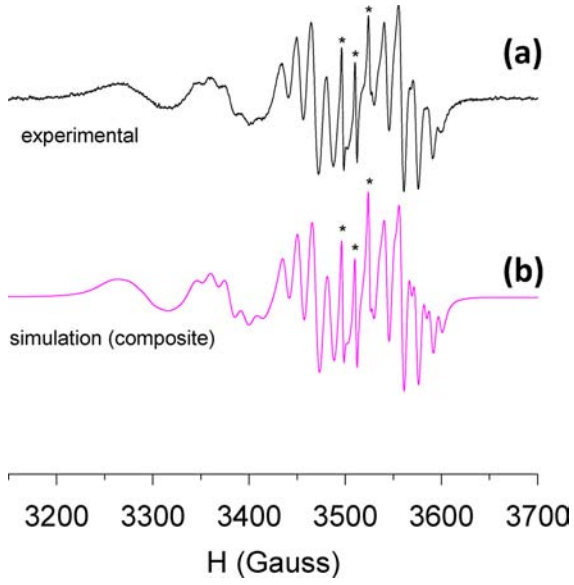

Figure 5. Experimental and simulated EPR spectra of $[Cu^{II}(ttfasbz)]^-$. (a) X-band (ν = 9.449 GHz) spectra (1 mM in DMF, 298 K) of $[Cu^{II}(ttfasbz)]^-$ prepared by reduction of the parent Cu^{III} complex with cobaltocene. Note the presence of a three line signal (*) due to a transient organic radical. (b) Composite computer simulation of the EPR spectra of $[Cu^{II}(ttfasbz)]^-$ plus the radical in a ratio of 1 (radical):1.8 (Cu^{II}).

Table 2. Spin Hamiltonian Parameters for $[Cu^{II}(ttfasbz)]$ and Related Compounds in Chart 2 (ND, Not Determined)

	$[Cu^{II}(ttfasbz)]^-$	$[Cu^{II}(phmi)]^{2-}$	$[Cu^{II}(cdMenappd)]$	$[Cu^{II}(salen)]$
g_x	2.0261	2.028	2.036	2.054
g_y	2.0263	2.035	2.053	2.054
g_z	2.1056	2.119	2.168	2.212
A_x (^{63}Cu) (10^{-4}cm^{-1})	37.32	36.8	ND	30.7
A_y (^{63}Cu) (10^{-4}cm^{-1})	27.90	35.2	25.0	30.7
A_z (^{63}Cu) (10^{-4}cm^{-1})	186.53	195.0	189.0	203.7
A_x (^{14}N) (10^{-4}cm^{-1})	15.43	12.6	ND	ND
A_y (^{14}N) (10^{-4}cm^{-1})	16.54	15.1	12.7	ND
A_z (^{14}N) (10^{-4}cm^{-1})	14.17	12.3	ND	ND
g_{iso}	2.055	2.06	2.084	2.0999
A_{iso} (^{63}Cu) (10^{-4}cm^{-1})	84.11	88.5	77.0	86.0
A_{iso} (^{14}N) (10^{-4}cm^{-1})	14.70	12.6	12.0	ND
	this work	ref 12	ref 53	ref 54

dx.doi.org/10.1021/ic302596h | *Inorg. Chem.* 2013, 52, 1650−1657

Table 3. Selected Bond Distances (Å) from the DFT (B3LYP) Geometry Optimized Structures of [Cu(ttfasbz)], $[Cu(ttfasbz)]^{-}$, and $[Cu(ttfasbz)]^{2-}$, Where *S* Is the Total Electron Spin Quantum Number and the Terms UKS and RKS Refer to the Use of Unrestricted and Restricted Kohn–Sham Approaches, Respectively

	[Cu(ttfasbz)]	$[Cu(ttfasbz)]^{-}$	$[Cu(ttfasbz)]^{2-}$
S	0	0.5	0
method	RKS	UKS	RKS
Cu–S(1)	2.22200	2.32066	2.41480
Cu–S(3)	2.22551	2.29366	2.36313
Cu–N(2)	1.93612	1.97010	2.09817
Cu–N(3)	1.95803	2.00254	2.15985
S(1)–C(1)	1.74203	1.73524	1.71822
C(1)–N(1)	1.29564	1.28753	1.29222
N(1)–N(2)	1.35162	1.37017	1.37403
N(2)–C(3)	1.34378	1.33097	1.33240
C(3)–C(5)	1.38520	1.39018	1.39878
C(5)–C(6)	1.41401	1.41490	1.42096
C(6)–N(3)	1.34471	1.33365	1.33117
N(3)–N(4)	1.34149	1.36335	1.35973
N(4)–C(7)	1.30275	1.29437	1.29791
C(7)–S(3)	1.73319	1.73239	1.71870

complexes where a change in bond order of the −HN−C═S moiety of the free ligand to an ene-thiolate −N═C−S^{-} occurs upon coordination. The loss of the proton from the thenoyltrifluoroacetone moiety is reminiscent of Schiff base complexes of ligands derived from acetylacetone, such as $(acacsme)^{3-}$ in Chart 1, where the central methylene group is acidic and takes on partial aromatic character once deprotonated.[11]

Electrochemistry. Cyclic voltammetry of $[Cu^{III}(ttfasbz)]$ revealed a variety of metal- and ligand-centered redox processes. Two quasi-reversible single-electron reductions were found at −126 mV vs $Fc^{+/0}$ and −1669 mV vs $Fc^{+/0}$ (Figure 2) when cycling within the potential window −2000 < E < +500 mV vs $Fc^{+/0}$. These are assigned to the $[Cu^{III/II}(ttfasbz)]^{0/-}$ and $[Cu^{II/I}(ttfasbz)]^{-/2-}$ couples on the basis of their potentials and stoichiometry. On sweeping to higher potentials, a multielectron irreversible anodic wave due to thiophene oxidation was seen. The multielectron nature of this process was not investigated further, but electropolymerization of thiophene monomers at similar potentials is a facile reaction, and similar chemistry is likely here. On the reverse sweep, an additional Cu-based response emerges at slightly lower potential (Figure 2, upper trace), which we tentatively assign to oligomeric complexes bridged by thiophene residues.

These results demonstrate that $[Cu^{III}(ttfasbz)]$ exhibits a $Cu^{III/II}$ redox potential similar to the ferrocenium/ferrocene couple so the trivalent form of the complex is only a mild oxidant. Cobaltocene under the same conditions yielded a reversible $[Co(cp)_2]^{+/0}$ redox response at −1400 mV vs $Fc^{+/0}$. This compound was thus an ideal reductant to generate the monoanion $[Cu^{II}(ttfasbz)]^{-}$ by chemical reduction (see below), while the monovalent complex was not accessible by chemical reduction ($Cu^{II/I}$ −1669 mV vs $Fc^{+/0}$). For comparison, the related Cu complexes of N_2S_2 bis-thiosemicarbazones of glyoxal (and analogs) reported by Donnelly et al.[52] exhibit $Cu^{II/I}$ couples at higher potentials (approximately in the range −1000 to −800 mV vs $Fc^{+/0}$ in DMSO). So, the extensive delocalization and extra negative charge of the ligand $ttfasbz^{3-}$ stabilize the Cu^{III} redox state by more than 600 mV at

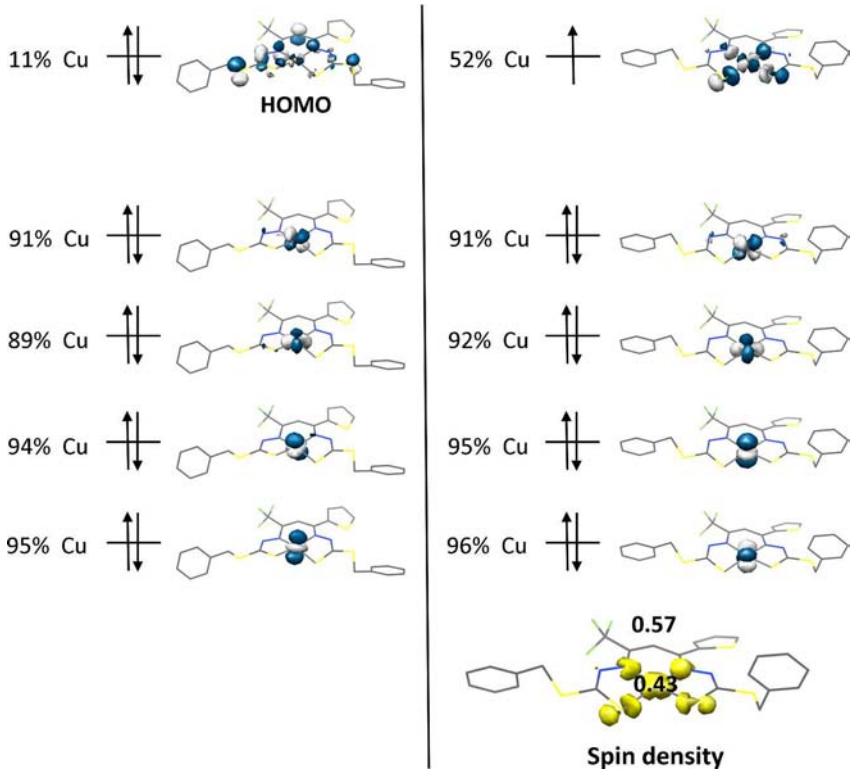

Figure 6. Qualitative frontier molecular orbital diagrams displaying the HOMO and orbitals of high Cu-character for [Cu(ttfasbz)] (left) and $[Cu(ttfasbz)]^{-}$ (right), plus a spin density plot and Mulliken spin population analysis for the latter. Note that the doubly occupied orbitals of dominant Cu character have been localized.

dx.doi.org/10.1021/ic302596h | *Inorg. Chem.* 2013, 52, 1650–1657

Scheme 2. Formal Oxidation States of [Cu(ttfasbz)] and Its One-Electron and Two-Electron Reduced Forms

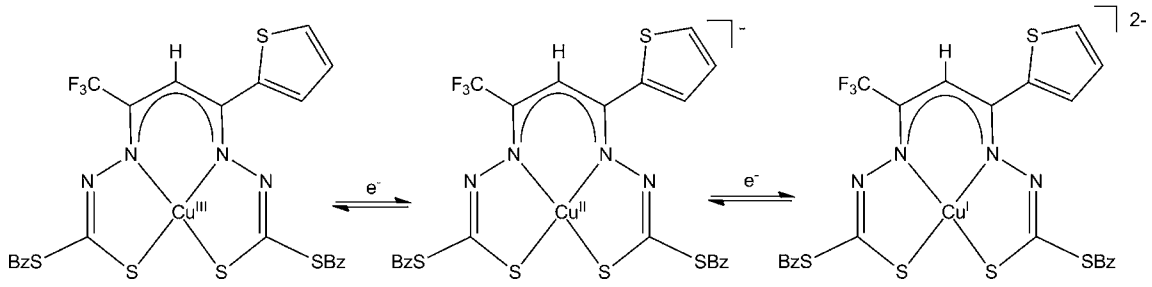

the expense of the Cu^{I} form. Although the low potential $Cu^{II/I}$ couple is totally reversible, we did not attempt to generate this monovalent complex either in bulk solution or in the solid state. On the basis of its redox potential, which is more than 250 mV lower than cobaltocene, it would be very oxygen sensitive.

EPR Spectroscopy. A freshly prepared solution of $[Cu^{III}(ttfasbz)]$ in DMF yielded a very weak frozen solution (140 K) EPR spectrum (Figure 3a, blue trace). In principle, the low spin trivalent (d^8) complex should be diamagnetic, but partial reduction by the solvent had occurred to generate a small amount of the paramagnetic $[Cu^{II}(ttfasbz)]^-$. This was confirmed by addition of an equivalent amount of $[Co(cp)_2]$, which resulted in significant enhancement of the Cu^{II} EPR spectrum (Figure 3b, black trace). It should be noted that both $[Co(cp)_2]$ and $[Co(cp)_2]^+$ are EPR silent. Quantitative reoxidation of the sample was achieved by addition of excess solid ferric chloride, which removed all Cu^{II} EPR signals (Figure 3c, red trace). The only detectable EPR signals were from trace Mn^{II} ($S = 5/2$, $I = 5/2$) impurities in the $FeCl_3$ oxidant, and these are seen as a weak sextet arising from the $I \pm 1/2\rangle$ Kramers doublet.

The anisotropic frozen solution EPR spectrum of $[Cu^{II}(ttfasbz)]^-$ is consistent with a pseudosquare planar Cu complex with a $d_{x^2-y^2}$ ground state. The spectrum is highly resolved, revealing hyperfine coupling to both ^{63}Cu and ^{65}Cu isotopes (Figure 4, low field "z" resonance) and superhyperfine coupling to the two N-donor atoms (^{14}N, I = 1, 99.632%; ^{15}N, I = 1/2, 0.368%), resulting in each Cu resonance being split into five dominant resonances from the ^{14}N nuclei.

Computer simulation of the anisotropic frozen solution EPR spectrum of $[Cu^{II}(ttfasbz)]^-$ with a rhombic spin Hamiltonian (eq 1)

$$H = \beta \cdot B \cdot g \cdot S + \sum_{^{63,65}Cu} (S \cdot A \cdot I - g_n \beta_n B \cdot I) + \sum_{^{14,15}N} \sum_{i=1}^{2} (S \cdot A_i \cdot I - g_n \beta_n B \cdot I) \quad (1)$$

was undertaken with the XSophe-Sophe-XeprView computer simulation suite[21] to determine the spin Hamiltonian parameters listed in Table 2. We employed the quadratic version of the Hooke and Jeeves optimization algorithm to optimize the spin Hamiltonian parameters through a comparison of the experimental and simulated spectra, which are shown in Figure 4. Interestingly, these spectra are highly resolved, revealing the ^{14}N superhyperfine coupling along the x, y, and z principle axes, which is also apparent in the anisotropic EPR spectra of $[Cu^{II}(phmi)]^{2+}$ (N_2S_2, Chart 2)[12] and $[Cu(cdMenappd)]$[53] (N_2SO) but not Cu^{II} complexes having an N_2O_2 coordination sphere such as $[Cu(salen)]$.[54] This reflects a greater spin density on the ligating nitrogen nuclei as a consequence of enhanced covalent bonding. The S-donor atoms are evidently important in this greater degree of coordinate bond covalency.

At room temperature, a simpler EPR spectrum was obtained (Figure 5a) comprising four resonances (from isotropic hyperfine coupling with the Cu nucleus) whose line widths vary as a function of the nuclear spin quantum number, a consequence of incomplete motional averaging of the g and A matrices (see the Experimental Section). Superposed on each of these resonances is a five-line isotropic pattern (relative intensities 1:2:3:2:1) arising from hyperfine coupling to two magnetically equivalent nitrogen nuclei coordinated to the Cu^{II} ion. An additional three resonances with narrow linewidths (highlighted with * symbols, Figure 5a) are present and characteristic of an isolated organic radical bearing an unpaired electron coupled to a single N nucleus ($g_{iso} = 2.0062$, $A_{iso} = 13.00 \times 10^{-4}$ cm^{-1}). Addition of the simulated spectra of the isolated radical and the Cu^{II} species in a ratio of 1 (radical):1.8 (Cu) yields a composite spectrum (Figure 5b) that is in very close agreement to the experimental spectrum.

The presence of this organic radical is almost certainly coupled with the redox reaction that led to the partially reduced "as prepared" species in Figure 3. In the absence of any other compounds, the radical must result from one-electron DMF oxidation by the EPR silent trivalent $[Cu^{III}(ttfasbz)]$. However, the EPR spectrum of this species is not that of the DMF radical cation, which is more complicated,[55] but must be from a DMF radical decomposition product. This radical decays over periods of days at room temperature to leave only the signal of the Cu^{II} complex (Figure S1 in the Supporting Information), so its identity remains unknown. This is consistent with the (stable) Cu^{II} EPR signal always being dominant of the radical, which eventually decays completely (Figure S1 in the Supporting Information).

Computational Studies. Although all evidence points to the isolated neutral complex having a formal trivalent Cu oxidation state, the ligand $ttfasbz^{3-}$ is potentially redox active (noninnocent). As a consequence, an alternative formulation of the neutral complex as containing a Cu^{II} ion coordinated to a ligand radical dianion, which strongly antiferromagnetically couple to one another to yield the observed $S = 0$ ground state, is also feasible. In an effort to differentiate between these two possible electronic structures, we undertook a DFT (B3LYP) computational analysis of the closed-shell $S = 0$ (Cu^{III}), open-shell $S = 0$ (Cu^{II}, plus ligand radical dianion), and $S = 1$ states of $[Cu(ttfasbz)]$ using the RKS, BS(1,1), and UKS formalisms, respectively. The structural parameters of the RKS geometry optimized structure (Table 3), which is ca. 2.5 kcal lower in energy than the corresponding $S = 1$ solution, display good

dx.doi.org/10.1021/ic302596h | Inorg. Chem. 2013, 52, 1650−1657

agreement with those of the X-ray crystal structure. Interestingly, the orientations of the thiophene and benzyl groups were well reproduced in the gas phase calculations, indicating they are not merely a consequence of crystal packing forces.

Efforts to geometry optimize using the BS(1,1) formalism yielded only RKS solutions. However, a BS(1,1) solution was obtained by performing a single point calculation using the atomic coordinates of the UKS $S = 1$ geometry optimized structure, but this was even higher in energy (ca. 3.5 kcal above the RKS solution). Furthermore, efforts to obtain a BS(1,1) solution using the true atomic coordinates (the X-ray crystal structure) were unsuccessful, and the singlet closed shell state was in this case calculated to be more than 10 kcal lower in energy than the triplet ($S = 1$) state. Hence, we can confidently rule out an electronic structure comprising a Cu^{II} ion coordinated to a ligand radical dianion and conclude that the closed shell solution containing Cu^{III} (see the four doubly occupied d orbitals in Figure 6) is the electronic ground state.

In addition, we have calculated the geometry-optimized and electronic structures of the mono- and dianions $[Cu(ttfasbz)]^{1-/2-}$. As expected, the C−C, C−N, N−N, and C−S bond distances for the respective $S = 1/2$ and $S = 0$ ground states (broken symmetry solutions could not be found in either case) are very similar to those determined and calculated for the neutral species. In contrast, the corresponding Cu−N and Cu−S bond lengths increase (Table 3) with increasing negative charge of the four coordinate species. This is a clear indication that reduction of the diamagnetic neutral complex to the mono- and dianion (Scheme 2) is predominantly a metal-centered process, so involve sequential reduction of Cu^{III} to Cu^{II} and then Cu^{II} to Cu^{I}. This is reflected in the qualitative frontier molecular orbital schemes for $[Cu^{III}(ttfasbz)]$, $[Cu^{II}(ttfasbz)]^{1-}$, and $[Cu^{I}(ttfasbz)]^{2-}$. High levels of covalency were seen in all frontier orbitals, and for the sake of formal oxidation state assignment, it was necessary to localize the occupied orbitals containing Cu d character. The latter contains five (see the Supporting Information) and the former two complexes (Figure 6) four doubly occupied orbitals with predominant Cu character. In addition, the monanion has a SOMO with only 52% Cu character, and a Mulliken spin density population analysis shows that the unpaired electron is evenly distributed over the metal ion and the ligand, both of which reflect the highly covalent bonding situation in this complex and also is consistent with the strong ^{14}N superhyperfine coupling apparent in the EPR spectra (Figures 3−5) between the N donor nuclei and the unpaired electron.

CONCLUSIONS

The highly conjugated trianion $(ttfasbz)^{3-}$ when coordinated as an N_2S_2 ligand stabilizes trivalent Cu. The $Cu^{III/II}$ redox potential of the complex is remarkably low (slightly lower than the ferrocenium/ferrocene couple), which has enabled its isolation and structural characterization. In fact, no oxidant was employed in the synthesis of $[Cu^{III}(ttfasbz)]$ from $[Cu^{II}(OAc)_2]$, so dioxygen appears to be the oxidant. Reduction of $[Cu^{III}(ttfasbz)]$ with cobaltocene generates $[Cu^{II}(ttfasbz)]^{-}$, which exhibits a characteristic axial EPR spectrum of a d^9 complex and further reduction to a formally monovalent (d^{10}) dianion $[Cu^{I}(ttfasbz)]^{2-}$, may be achieved electrochemically. The cyclization reaction leading to the pyrazoline H_3ttfasbz is evidently reversible as complexation reactions starting with this cyclic compound progress in a facile manner. The stabilization of Cu in three different oxidation states is quite remarkable, and our computational and spectroscopic results indicate that the three oxidation state changes are truly metal centered, and this potentially noninnocent ligand does not undergo any redox reactions. The role of the $-CF_3$ and thiophene substituents in stabilizing this unusual oxidation state remains unclear, and studies on analogues derived from acetylacetone are warranted.

ASSOCIATED CONTENT

Supporting Information

Figures of EPR spectra, DFT calculated spin density plots and Mulliken populations, and qualitative frontier molecular orbital diagram; tables of the energies of the calculated $[Cu(ttfasbz)]^n$ species and DFT geometry optimized atomic *xyz* coordinates; and .cif file. This material is available free of charge via the Internet at http://pubs.acs.org.

AUTHOR INFORMATION

Corresponding Author

*E-mail: p.bernhardt@uq.edu.au.

Notes

The authors declare no competing financial interest.

ACKNOWLEDGMENTS

We gratefully acknowledge financial support from the University of Queensland and the Max Planck Society for granting a fellowship to J.E.

REFERENCES

(1) Diaddario, L. L.; Robinson, W. R.; Margerum, D. W. *Inorg. Chem.* **1983**, *22*, 1021−1025.
(2) McDonald, M. R.; Fredericks, F. C.; Margerum, D. W. *Inorg. Chem.* **1997**, *36*, 3119−3124.
(3) Pratesi, A.; Zanello, P.; Giorgi, G.; Messori, L.; Laschi, F.; Casini, A.; Corsini, M.; Gabbiani, C.; Orfei, M.; Rosani, C.; Ginanneschi, M. *Inorg. Chem.* **2007**, *46*, 10038−10040.
(4) Bossu, F. P.; Chellappa, K. L.; Margerum, D. W. *J. Am. Chem. Soc.* **1977**, *99*, 2195−2203.
(5) Maeda, H.; Ishikawa, Y.; Matsuda, T.; Osuka, A.; Furuta, H. *J. Am. Chem. Soc.* **2003**, *125*, 11822−11823.
(6) Will, S.; Lex, J.; Vogel, E.; Schmickler, H.; Gisselbrecht, J.-P.; Haubtmann, C.; Bernard, M.; Gorss, M. *Angew. Chem., Int. Ed. Engl.* **1997**, *36*, 357−361.
(7) Brückner, C.; Briñas, R. P.; Krause Bauer, J. A. *Inorg. Chem.* **2003**, *42*, 4495−4497.
(8) Cervera, B.; L. Sanz, J.; J. Ibanez, M.; Vila, G.; Lloret, F.; Julve, M.; Ruiz, R.; Ottenwaelder, X.; Aukauloo, A.; Poussereau, S.; Journaux, Y.; Carmen Munoz, M. *J. Chem. Soc., Dalton Trans.* **1998**, 781−790.
(9) Krebs, C.; Glaser, T.; Bill, E.; Weyhermüller, T.; Meyer-Klaucke, W.; Wieghardt, K. *Angew. Chem., Int. Ed.* **1999**, *38*, 359−361.
(10) Oliver, K. J.; Waters, T. N. *J. Chem. Soc., Chem. Commun.* **1982**, 1111−1112.
(11) Knof, U.; Weyhermüller, T.; Wolter, T.; Wieghardt, K. *J. Chem. Soc., Chem. Commun.* **1993**, 726−728.
(12) Hanss, J.; Krüger, H.-J. *Angew. Chem., Int. Ed. Engl.* **1996**, *35*, 2827−2830.
(13) Desbenoit, N.; Galardon, E.; Roussel, P.; Artaud, I.; Tomas, A. *J. Coord. Chem.* **2009**, *62*, 2472−2479.
(14) Butin, K. P.; Beloglazkina, E. K.; Zyk, N. V. *Russ. Chem. Rev.* **2005**, *74*, 531−553.
(15) Kaim, W. *Inorg. Chem.* **2011**, *50*, 9752−9765.
(16) Ghosh, M.; Weyhermüller, T.; Wieghardt, K. *Dalton Trans.* **2010**, *39*, 1996−2007.
(17) Brown, S. N. *Inorg. Chem.* **2012**, *51*, 1251−1260.

(18) Gerbeleu, N. V.; Simonov, Y. A.; Arion, V. B.; Leovac, V. M.; Turta, K. I.; Indrichan, K. M.; Gradinaru, D. I.; Zavodnik, V. E.; Malinovskii, T. I. *Inorg. Chem.* **1992**, *31*, 3264−3268.
(19) Knof, U.; Weyhermüller, T.; Wolter, T.; Wieghardt, K.; Bill, E.; Butzlaff, C.; Trautwein, A. X. *Angew. Chem., Int. Ed. Engl.* **1993**, *32*, 1635−1638.
(20) Akbar Ali, M.; Tarafdar, M. T. H. *J. Inorg. Nucl. Chem.* **1977**, *39*, 1785−1791.
(21) Hanson, G. R.; Gates, K. E.; Noble, C. J.; Griffin, M.; Mitchell, A.; Benson, S. *J. Inorg. Biochem.* **2004**, *98*, 903−916.
(22) Kivelson, D. *J. Chem. Phys.* **1960**, *33*, 1094−1106.
(23) Atkins, P. W.; Kivelson, D. *J. Chem. Phys.* **1966**, *44*, 169−174.
(24) Wilson, R.; Kivelson, D. *J. Chem. Phys.* **1966**, *44*, 154−168.
(25) Wilson, R.; Kivelson, D. *J. Chem. Phys.* **1966**, *44*, 4440−4444.
(26) Froncisz, W.; Hyde, J. S. *J. Chem. Phys.* **1980**, *73*, 3123−3131.
(27) Hyde, J. S.; Froncisz, W. *Annu. Rev. Biophys. Bioeng.* **1982**, *11*, 391−417.
(28) Sheldrick, G. M. *Acta Crystallogr., Sect. A* **2008**, *A64*, 112−122.
(29) Farrugia, L. J. *J. Appl. Crystallogr.* **1997**, *30*, 565.
(30) Neese, F. *ORCA, an Ab Initio, Density Functional and Semiempirical Electronic Structure Package*, vers. 2.8; Universität Bonn: Bonn, Germany, 2010.
(31) Becke, A. D. *J. Chem. Phys.* **1986**, *84*, 4524−4529.
(32) Becke, A. D. *J. Chem. Phys.* **1993**, *98*, 5648−5652.
(33) Lee, C. T.; Yang, W. T.; Parr, R. G. *Phys. Rev. B: Condens. Matter Mater. Phys.* **1988**, *37*, 785−789.
(34) Weigend, F.; Alrichs, R. *Phys. Chem. Chem. Phys.* **2005**, *7*, 3297−3305.
(35) Eichkorn, K.; Weigend, F.; Treutler, O.; Ahlrichs, R. *Theor. Chem. Acc.* **1997**, *97*, 119−124.
(36) Eichkorn, K.; Treutler, O.; Öhm, H.; Häser, M.; Ahlrichs, R. *Chem. Phys. Lett.* **1995**, *240*, 283−290.
(37) Kossmann, A. S.; Neese, F. *Chem. Phys. Lett.* **2009**, *481*, 240−243.
(38) Neese, F.; Wennmohs, F.; Hansen, A.; Becker, U. *Chem. Phys.* **2009**, *356*, 98−109.
(39) Klamt, A.; Schüürmann, G. *J. Chem. Soc. Perkin Trans. 2* **1993**, 799−805.
(40) Grimme, A. S. *J. Comput. Chem.* **2006**, *27*, 1787−1799.
(41) Noodleman, L.; Peng, C. Y.; Case, D. A.; Mouesca, J. M. *Coord. Chem. Rev.* **1995**, *144*, 199−244.
(42) Kirchner, B.; Wennmohs, F.; Ye, S.; Neese, F. *Curr. Opin. Chem. Biol.* **2007**, *11*, 134−141.
(43) Neese, F. *J. Phys. Chem. Solids* **2004**, *65*, 781−785.
(44) Pettersen, E. F.; Goddard, T. D.; Huang, C. C.; Couch, G. S.; Greenblatt, D. M.; Meng, E. C.; Ferrin, T. E. *J. Comput. Chem.* **2004**, *25*, 1605−12.
(45) Iskander, M. F.; El-Sayed, L.; El-Toukhy, A.; Tawflk, M. *Transition Met. Chem.* **1982**, *7*, 135−140.
(46) Du Preez, J. G. H.; Gerber, T. I. A.; Knoesen, O. *Inorg. Chim. Acta* **1987**, *133*, 3−5.
(47) Gerber, T. I. A.; Hosten, E.; Knoesen, O.; Mayer, P. *J. Coord. Chem.* **2007**, *60*, 2369−2375.
(48) Akbar Ali, M.; Mirza, A.; Butcher, R.; Chowdhury, A. *Transition Met. Chem.* **2011**, *36*, 471−479.
(49) Castiñeiras, A.; Bermejo, E.; West, D. X.; El-Sawaf, A. K.; Swearingen, J. K. *Polyhedron* **1998**, *17*, 2751−2757.
(50) Cowley, A. R.; Dilworth, J. R.; Donnelly, P. S.; Gee, A. D.; Heslop, J. M. *Dalton Trans.* **2004**, 2404−2412.
(51) Calatayud, D. G.; López-Torres, E.; Mendiola, M. A.; Pastor, C. J.; Procopio, J. R. *Eur. J. Inorg. Chem.* **2005**, *2005*, 4401−4409.
(52) Xiao, Z.; Donnelly, P. S.; Zimmermann, M.; Wedd, A. G. *Inorg. Chem.* **2008**, *47*, 4338−4347.
(53) Pereira, E.; Gomes, L. R.; Low, J. N.; de Castro, B. *Polyhedron* **2008**, *27*, 335−343.
(54) Bhadbhade, M. M.; Srinivas, D. *Inorg. Chem.* **1993**, *32*, 6122−6130.
(55) Eastland, G. W.; Rao, D. N. R.; Symons, M. C. R. *J. Chem. Soc., Faraday Trans.* **1986**, *82*, 2833−2842.